

WHALES: A Multi-agent Scheduling Dataset for Enhanced Cooperation in Autonomous Driving

Siwei Chen[†], Yinsong (Richard) Wang[†], Ziyi Song, Sheng Zhou*

Abstract—Achieving high levels of safety and reliability in autonomous driving remains a critical challenge, especially due to occlusion and limited perception ranges in stand-alone systems. Cooperative perception among vehicles offers a promising solution, but existing research is hindered by datasets with a limited number of agents. Scaling up the number of cooperating agents is non-trivial and introduces significant computational and technical hurdles that have not been addressed in previous works. To bridge this gap, we present Wireless enHanced Autonomous vehicles with Large number of Engaged agentS (WHALES), a dataset generated using CARLA simulator that features an unprecedented average of 8.4 agents per driving sequence. In addition to providing the largest number of agents and viewpoints among autonomous driving datasets, WHALES records agent behaviors, enabling cooperation across multiple tasks. This expansion allows for new supporting tasks in cooperative perception. As a demonstration, we conduct experiments on agent scheduling task, where the ego agent selects one of multiple candidate agents to cooperate with, optimizing perception gains in autonomous driving. The WHALES dataset and codebase can be found at <https://github.com/chensiweiTHU/WHALES>.

I. INTRODUCTION

Autonomous Driving (AD) technology holds the promise of preventing traffic accidents, enhancing mobility for disabled individuals, and improving overall traffic safety and efficiency. Recent advancements in deep learning have brought significant breakthroughs to AD technologies in various perception tasks such as 3D object detection [1], 4D occupancy prediction [2], multi-object tracking [3], and end-to-end planning [4]. To navigate through complex surrounding environment, AD systems utilize different sensor arrays, such as cameras, LiDARs, radars and IMU, to perceive their surroundings and make impactful decisions on ego-vehicle behavior.

Howeve, stand-alone or single-vehicle AD systems face a critical limitation in perception: their inability to detect information from Non-Line-Of-Sight (NLOS) regions, leading to significant occlusions that pose potential safety risk. To overcome this, researchers have introduced cooperative driving through wireless communication, which enhances safety, particularly in complex and challenging road scenarios. The NR-V2X technology outlined by 3GPP in Releases 17 and 18 [5] supports raw, feature and object-level fusion in cooperative driving, enabling cooperation under groupcast

and unicast modes. These cooperative driving strategies, which enables collaboration between connected autonomous vehicles (CAV) and roadside units (RSU), pave the way for safer and more efficient autonomous transportation systems.

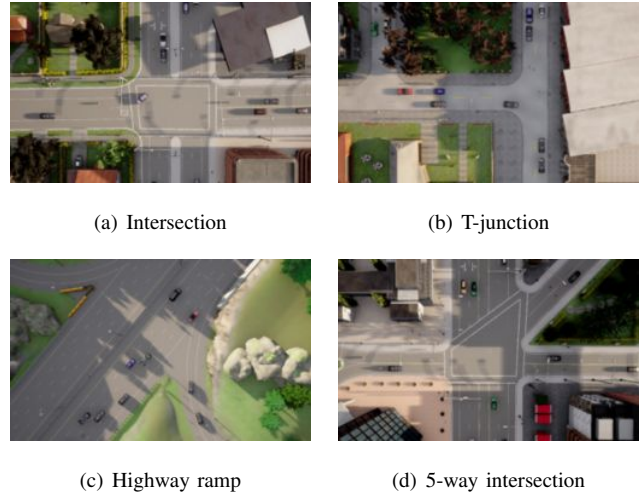


Fig. 1: The four road scenes from the WHALES dataset. These scenes were generated using various CARLA towns, and different agent and spawning configurations.

Several studies [6]–[10] have focused on enhancing the robustness of cooperative perception (CP) by addressing challenges posed by non-ideal factors in the fields of autonomous driving and communication, such as communication latency, sensor localization errors, and various communication constraints. In these studies, intelligent agents improve perception at different stages of the model: raw sensory data is fused in early fusion, processed encoded features are combined in intermediate fusion and detection results are integrated in late fusion [11], which leads to improved average precision [6] [7] [10]. Other research efforts [8] [9] [12] aim to enhance cooperative perception by modeling the non-ideal factors that arise when autonomous driving systems are combined with communication, ensuring that the proposed models remain robust under these conditions.

To promote innovative research in cooperative autonomous driving, we introduce a multi-agent scheduling dataset, namely **Wireless enHanced Autonomous vehicles with Large number of Engaged agentS (WHALES)**, which covers 70K RGB images, 17K LiDAR frames and 2.01M 3D bounding box annotations. As shown in Fig. 1, WHALES features

[†] Equal contribution.

* Sheng Zhou is the corresponding author of this paper.

Email: sheng.zhou@tsinghua.edu.cn

The authors are with Tsinghua University, Beijing, P.R. China.

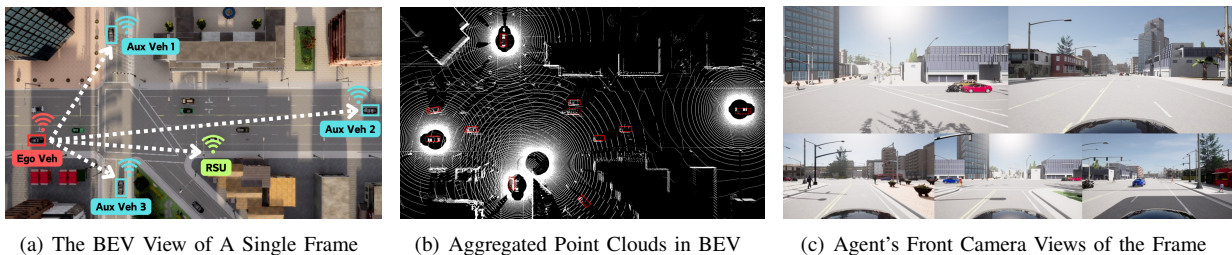


Fig. 2: An overview of the proposed WHALES dataset. (a) Bird’s-eye view (BEV) of a single frame from the dataset. (b) Visualization of point clouds and bounding boxes in the BEV view. (c) Agent’s front camera views of the frame.

various road scenarios, including intersections, T-junctions, highway ramps, roundabout, and 5-way intersections. It goes beyond conventional perception-based approaches to enable more comprehensive cooperative functionalities. Our dataset and benchmarking tasks are specifically designed to foster innovation and drive progress in V2X cooperative perception.

Fig. 2 provides an overview of a single frame from the WHALES dataset. In Fig. 2(a), the bird’s-eye view (BEV) of the scenario is shown. Fig. 2(b) visualizes the point clouds from all agents, including one RSU, within the frame, while the Fig. 2(c) shows the front camera views of all agents. The ego vehicle can detect surrounding objects by properly scheduling cooperation with nearby agents.

Experiments conducted on the WHALES dataset cover stand-alone and cooperative 3D perception, as well as agent scheduling. Agent scheduling, a new task introduced by our dataset, extends beyond what has been explored in previous research. We implement the dataset using MMDetection3D [13] and provide baseline models along with corresponding performance metrics. Existing agent scheduling methods are incorporated into preprocessing pipelines, enabling researchers to easily propose and evaluate new scheduling strategies. Our contributions can be summarized as follows:

- 1) We build WHALES, a large-scale scheduling dataset supporting V2V and V2I perception. By significantly optimizing the simulation speed and computation cost of CARLA when handling a large number of agents, all the scenes are generated with multi-modal sensors and features an average of 8.4 agents per driving sequence. Our dataset includes more than 2.01M annotated 3D bounding boxes, along with object indices and agent behavior information, allowing for strong extensibility to downstream tasks.
- 2) We illustrate the applications of our dataset on two cooperative tasks, including 3D object detection and agent scheduling. To our knowledge, this is the first dataset to consider scheduling in cooperative perception. We provide detailed benchmarks for both tasks, and for agent scheduling, we provide analysis on various existing single-agent and multi-agent scheduling algorithms.

II. RELATED WORK

Large open datasets play an essential role to advancing collaborative perception in autonomous driving systems. Earlier works, including KITTI [14], nuScenes [15] and Waymo Open [21], provide real-world scenarios supporting tasks like 3D object detection and tracking. For motion forecasting and planning, Argoverse [22] and Argoverse2 [23] datasets offer valuable data, including tracking and motion forecasting annotations, and semantic metadata. Additionally, the nuPlan [24] dataset introduces a closed-loop, machine-learning-based planning benchmark. However, these datasets are limited to single-vehicle scenarios, restricting their applicability for collaborative perception due to the limited perceptual fields of individual vehicles.

To address this limitation, Vehicle-to-Everything (V2X) perception has emerged as a solution. By enabling information exchange between vehicles or with roadside units, V2X perception significantly enhances the capability of autonomous vehicles to handle challenging conditions such as occlusions and long-range perception. In the realm of real-world datasets, DAIR-V2X [16] stands out as the first large-scale dataset dedicated to collaborative perception for 3D object detection. Additionally, V2V4Real [20] offers data from two vehicles equipped with LiDARs and cameras, facilitating 3D object detection and tracking. The V2X-Seq [25] dataset expands the resource pool by providing comprehensive sequential data frames, trajectories, vector maps, and traffic light information from real-world settings. While numerous real-world datasets have emerged, the scale of datasets specifically designed for cooperative perception remains constrained for various reasons. For instance, datasets like DAIR-V2X [16] and V2X-Seq [25] are geographically limited to Beijing, China.

Due to the challenges of collecting real-world data, simulation-based approaches have gained popularity in generating collaborative perception datasets. OPV2V [18] is a significant development in this area, being the first large-scale simulated dataset for Vehicle-to-Vehicle (V2V) perception. It encompasses diverse environments, including eight towns within the CARLA [26] simulator and a digital representation of Culver City. V2X-Sim [17] extends this by supporting both V2V and Vehicle-to-Infrastructure (V2I) perception. Additionally, DOLPHINS [19] contributes to the field by enabling V2V and V2I perceptions, introducing a

TABLE I: A Detailed Comparison Between Proposed Dataset and Existing Autonomous Driving Datasets

Dataset	Year	Real/Simulated	V2X	Image	Point Cloud	3D Annotations	Classes	Average No. of Agents
KITTI [14]	2012	real	No	15k	15k	200k	8	1
nuScenes [15]	2019	real	No	1.4M	400k	1.4M	23	1
DAIR-V2X [16]	2021	real	V2V&I	39k	39k	464k	10	2
V2X-Sim [17]	2021	simulated	V2V&I	0	10k	26.6k	2	2
OPV2V [18]	2022	simulated	V2V	44k	11k	230k	1	3
DOLPHINS [19]	2022	simulated	V2V&I	42k	42k	293k	3	3
V2V4Real [20]	2023	real	V2V	40k	20k	240k	5	2
WHALES (Ours)	2024	simulated	V2V&I	70k	17k	2.01M	3	8.4

TABLE II: Sensor specifications for CAVs and RSUs

Sensors	Details
4x Camera	RGB, Tesla: 1920×1080
1x LiDAR	64 channels, 256k points per second, 200m capturing range, -40° to 0° vertical FOV, 20Hz

broader range of scenarios with dynamic weather conditions.

While simulators offer advantages in generating cooperative perception datasets, there are still limitations regarding the number of agents included. This limitation arises from the high computational demands involved in simulating detailed sensor data and complex interactions among many vehicles simultaneously. Additionally, real-world datasets are often constrained by economic factors, typically featuring only two viewpoints, while simulated datasets offer only a few more. For instance, DOLPHINS [19] and OPV2V [18] contain an average of three viewpoints per scene, supporting V2V perception. Most existing datasets are primarily designed for perception tasks, with limited scene lengths, and they rely solely on CARLA auto-pilot system for planning and control.

Most existing datasets assume ideal conditions for cooperative perception. The mobility-aware sensor scheduling (MASS) [27] algorithm addresses decentralized sensor scheduling by using vehicle dynamics to maximize the ego vehicle’s perception gain. MASS leverages the Upper Confidence Bound (UCB) [28] approach to adapt to V2X environments, adjusting confidence bounds based on historical data.

III. WHALES DATASET

Table I highlights the strengths of our dataset over existing cooperative perception datasets. WHALES offers several unique advantages, including the extensive support for V2V and V2I, and rich road information through a large number of viewpoints per scene. With an average of 8.4 viewpoints per scene, our dataset surpasses others in its capability to evaluate the performance of different multi-agent scheduling algorithms. WHALES contains 17K LiDAR point clouds and 70K images, and its scenes exhibit a higher density of agents compared to other datasets. We defined a valid 3D bounding box as one that is within 50 meters of an agent’s view. By this definition, there are 2.01M valid 3D bounding boxes across multiple views. There are a total of 511K unique 3D bounding boxes across frames in the dataset, exceeding the number present in other existing datasets.

As the number of agents increases in a confined area, the simulation time and computational cost grows non-linearly

due to the increase in agent-wise interactions. To address this challenge, we assign a separate process for each active agent to generate raw data, storing the results in a queue. We ensure these agent processes are synchronized, and their observations are collated into batches. An expert model is then used to generate the agent behaviors simultaneously from the batch observations. On average, our simulator requires approximately 160ms per additional agent on an NVIDIA 4090 GPU, effectively reducing the time cost to a linear function, making the time and computational cost acceptable for dataset generation.

A. Sensor and Agent Settings

Table II and III outlines the sensor and agent configurations in the WHALES dataset. The dataset provides multi-modal sensory input for the intelligent agents, balancing complexity with the tasks supported by the simulator. In total, we define four types of agent. The first type of agent is the uncontrolled CAVs. The second type of agent is the controlled CAVs. Both types of CAVs are equipped with one 64-beam LiDAR and four 1920×1080 cameras, alongside with V2X communication devices. With the setup, they can perform perception and communication tasks. Controlled vehicles can be controlled through self-defined planning and control algorithms. The third type is the RSU installed on the roadside, also equipped with LiDARs and cameras. The fourth type is the non-player or obstacle agents, which do not have any sensors attached and have uncontrolled trajectories. Under this setup, we are able to evaluate the enhancement of safety and other benchmarks of AD contributed by cooperation.

B. Dataset Structure

Our dataset is organized into scenes, frames, samples and annotations. A scene represents a segment of the simulation. In the simulation, we set the sampling interval to 0.1 seconds, while one frame is saved every 0.5s. For every scene, we provide the basic simulation configuration information and two videos: one shows the front camera views of all agents, while the other presents an encoded BEV map similar to that in [29]. Within every frame, the object class, location, rotation and velocity of every agent are recorded along with annotations in the world coordinate system. In one frame, each agents plays the role of ego vehicle in turn, thus we have M samples per frame in a scenario with M intelligent agents. We project bounding boxes into ego vehicles’ coordinate

TABLE III: Four Classes of Agents in the WHALES Dataset

Agent Location	Agent Category	Sensor Configuration	Planning & Control	Tasks	Spawning Positions
On-Road	Uncontrolled CAV	LiDAR \times 1 + Camera \times 4	CARLA Auto-pilot	Perception	Random, deterministic
	Controlled CAV	LiDAR \times 1 + Camera \times 4	RL Algorithm	Perception & Planning	Random, deterministic
Roadside	RSU	LiDAR \times 1 + Camera \times 4	RL Algorithm	Perception & Planning	Static
Anywhere	Obstacle Agent	No sensors equipped	CARLA Auto-pilot	No tasks	Random

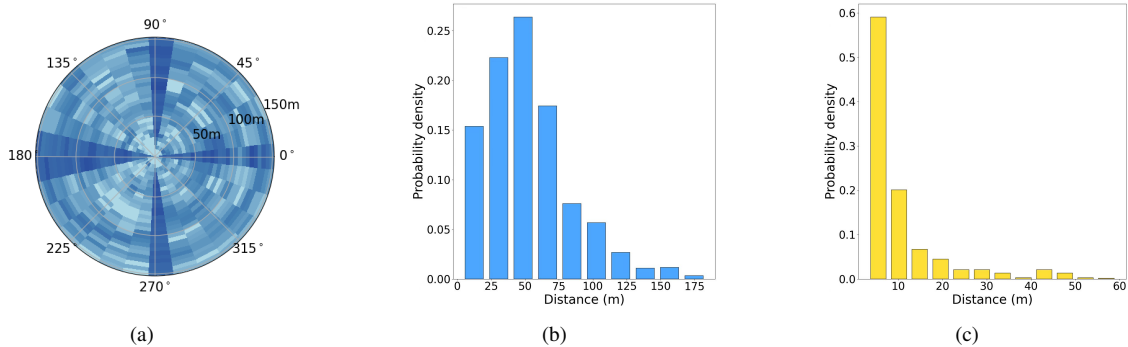


Fig. 3: (a) The distribution of bounding boxes in a polar density map on a logarithmic scale. (b) The distance between different cooperative agents. (c) The minimum distance between agents and objects.

systems and filter valid boxes within perception range to generate annotations in one sample.

C. Dataset Configuration System

We generate the dataset using a modified version CARLA Simulator [26]. Additionally, we inherit a reinforcement learning environment from [29], which includes some of the fundamental world settings from [30]. To create an environment conducive to cooperation, all agents are spawned within a rectangular area surrounding a central point. Our experimental configuration system is integrated in MMDetection3D [13], which utilizes a Python file to store experimental settings including model structure, data processing pipelines and agent scheduling policies.

D. Data Analysis

Fig. 3 display the orientations of the bounding box annotations in our dataset. As shown in Fig. 3(a), the bounding boxes surrounding the ego vehicle are distributed across various orientations. Due to the constraints of road orientation, many objects are aligned either parallel or perpendicular to the ego vehicle’s direction, showing a concentrated shade of blue in the four directions.

Fig. 3(b) shows the distribution of the distance between cooperative agents. Most vehicles are positioned close to one another, providing complementary viewpoints, while some are placed farther apart to offer long-range information. Fig. 3(c) illustrates the distribution of the minimum distances between agents and objects, with the closest objects typically within 20 meters of the agent.

Our annotation scheme follows the conventions of the nuScenes dataset [15]. It is important to note that all annotations are generated using the CARLA simulator [26]. The model is expected to detect all objects within the valid detection range of 50 meters, including occluded objects.

In addition to existing nuScenes labels, new annotations for cooperative perception tasks are included, such as graphs depicting the distance and occlusion relationships between agents.

E. Supported Tasks

The WHALES dataset supports both stand-alone and cooperative 3D object detection tasks. In cooperative driving, optimizing the scheduling of agents is a key focus of our work. Selecting the right agent for cooperation is crucial for training and inference in our dataset, which features a large number of candidates. This task is less relevant in existing dataset with fewer candidates. The agent scheduling procedure is integrated into the data preprocessing pipelines, with multiple scheduling algorithms available, allowing researchers to easily train and test different scheduling policies. In addition, we record ground-truth agent behaviors and trajectories of RL experts [29]. The scenes generated by the RL model are then filtered based on reward, scene length and the number of agents from three categories in the scene. This facilitates future extension for downstream tasks. In the following subsection, the implementation of each task will be introduced in details.

IV. EXPERIMENTS

We conduct experiments on cooperative tasks in autonomous driving, including stand-alone and cooperative 3D object detection, and agent scheduling. Various metrics are used for evaluating the performance of models on different tasks in our experiment. These benchmarks of each task will be introduced in the subsections below respectively.

A. Experimental Details

All models are trained on 8 NVIDIA GeForce RTX 3090 GPUs. For each task, our dataset is split with an 8:2 ratio

TABLE IV: Stand-alone 3D Object Detection Benchmark (50m/100m)

Method	$AP_{Veh} \uparrow$	$AP_{Ped} \uparrow$	$AP_{Cyc} \uparrow$	mAP \uparrow	mATE \downarrow	mASE \downarrow	mAOE \downarrow	mAVE \downarrow	NDS \uparrow
Pointpillars [31]	67.1 /41.5	38.0/6.3	37.3 /11.6	47.5/19.8	0.117/0.247	0.876/0.880	1.069 / 1.126	1.260/1.625	33.8/18.6
SECOND [32]	58.5/38.8	27.1/12.1	24.1/ 12.9	36.6/21.2	0.106/0.156	0.875/0.878	1.748/1.729	1.005 / 1.256	28.5/20.3
RegNet [33]	66.9/ 42.3	38.7/8.4	32.9/11.7	46.2/20.8	0.119/0.240	0.874 /0.881	1.079/1.158	1.231/1.421	33.2/19.2
VoxelNeXt [34]	64.7/ 42.3	52.2 / 27.4	35.9/9.0	50.9 / 26.2	0.075 / 0.142	0.877/ 0.877	1.212/1.147	1.133/1.348	36.0 / 22.9

TABLE V: Cooperative 3D Object Detection Benchmark (50m/100m)

Method	$AP_{Veh} \uparrow$	$AP_{Ped} \uparrow$	$AP_{Cyc} \uparrow$	mAP \uparrow	mATE \downarrow	mASE \downarrow	mAOE \downarrow	mAVE \downarrow	NDS \uparrow
No Fusion	67.1/41.5	38.0/6.3	37.3/11.6	47.5/19.8	0.117/0.247	0.876/0.880	1.069/ 1.126	1.260 /1.625	33.8/18.6
F-Cooper [35]	75.4 / 52.8	50.1/9.1	44.7/20.4	56.8/27.4	0.117/0.205	0.874 /0.879	1.074/1.206	1.358/ 1.449	38.5/22.9
Raw-level Fusion	71.3/48.9	38.1/8.5	40.7/16.3	50.0/24.6	0.135/0.242	0.875/0.882	1.062 /1.242	1.308/1.469	34.9/21.1
VoxelNeXt [34]	71.5/50.6	60.1 / 35.4	47.6 / 21.9	59.7 / 35.9	0.085 / 0.159	0.877/ 0.878	1.070/1.204	1.262/1.463	40.2 / 22.6

for training and testing. All models are trained for 24 epochs with a base learning rate of 0.001. We train and test models under detection ranges of 50m and 100m. The data volume of transmission is limited to 2MB per frame.

B. Stand-alone 3D Object Detection

Our models are implemented using the MMDetection3D [13] architecture. Most settings were consistent with the experimental setup used for the nuScenes dataset [15]. Specifically, we conduct experiments on three mainstream models, including Pointpillars [31], RegNet [33] and SECOND [32], to detect objects within the distances of 50m and 100m. The data augmentation procedures are the same as those used for models trained on the nuScenes [15] Dataset.

The benchmarks for 3D object detection are similar to those of nuScenes [15]. The weighted sum of **mAP** (mean Average Precision), **mATE** (mean Absolute Trajectory Error), **mASE** (mean Absolute Scale Error), **mAOE** (mean Absolute Orientation Error), **mAVE** (mean Absolute Velocity Error), **mAAE** (mean Absolute Attribute Error) are used to calculate the **NDS** (nuScenes Detection Score). Since the classes of objects are not divided into attributes, mAAE is preset to 1.

Table IV shows the results of stand-alone 3D object detection experiments in the 50m and 100m settings. All models perform better at detecting vehicles than at detecting cyclists and pedestrians, which is due to the larger average bounding box of vehicles compared to the other two classes. There is a significant drop in performance when the detection range is expanded to 100 meters, with most stand-alone perception models struggling to detect pedestrians and cyclists at this distance. These findings underscore the importance of cooperation in enhancing long-range perception.

C. Cooperative 3D Object Detection

We conduct experiments using mainstream models of CP. We use Pointpillars [31] for our baseline method. The implemented models share the preprocessing layers, backbone and head by default. In this subsection, all the agents choose one random agent to cooperate with during training and the closest agent during inference. While this basic approach already improves perception, the availability of more agents for the ego agent can significantly increase its perception

accuracy. A more comprehensive study on scheduling policy with more available candidate agents will be studied in the next subsection.

Table V present the experiment results for cooperative 3D object detection. We set the No Fusion method as our baseline, and find that the cooperative version of VoxelNeXt [34] with sparse convolution for fusion ranks highest among all single-level fusion models. All levels of cooperation can improve the detection performance comparing to the baseline. The raw-level CP is outperformed by feature-level methods because it shares the same model structure with no fusion approach with a weaker representational ability. Comparing to the baseline, F-Cooper [35] improves the mAP by 19.5% and 38.4% while the VoxelNeXt [34] has an improvement by 25.7% and 81.3% under 50m and 100m. The experimental results indicates a strong improvement of detection by cooperation.

D. Agent Scheduling

As shown in Fig. 4, in a typical scheduling task, the ego vehicle selects an agent from the candidate cooperative agents in unicast communication setting for raw-level fusion. In scenarios involving M agents, there are 2^M possible combinations of sensory inputs. Iterating over all possible combinations during the training phase is infeasible, making the selection of effective training and testing policies of CP models a non-trivial task. We present experiments conducted to evaluate various scheduling policies for training and inference in cooperative perception models. Models are trained under difference scheduling policies with the same model settings.

The **Full Communication** algorithm allows the ego agent to acquire point clouds from all other agents, representing an idealistic scenario and serving as the upper bound of perception performance, while **No Fusion** method corresponds to the lower bound. The **Closest Agent** algorithm, a more straightforward approach, selects the nearest agent without relying on any historical information. Other algorithms leverage historical rewards when performing scheduling. The **Historical Best** algorithm selects the candidate vehicle that provided the highest number of bounding boxes in ego vehicle’s range in the last frame. This can be implemented via a hand-shaking mechanism: the ego agent sends its

TABLE VI: mAP Scores on 3D Object Detection using Different Scheduling Policies (50m/100m)

Inference \ Training	No Fusion	Closest Agent	Single Random	Multiple Random	Full Communication
	Single-Agent Scheduling				
No Fusion	50.9/26.2	50.9/23.3	51.3/25.3	50.3/22.9	45.6/18.8
Closest Agent	39.9/20.3	58.4/30.2	58.3/32.6	57.7/30.5	55.4/10.8
Single Random	43.3/22.8	57.9/31.0	58.4/33.3	57.7/31.4	55.0/14.6
MASS [27]	55.5/11.0	58.8/33.7	58.9/34.0	57.3/32.3	54.1/27.4
Historical Best	54.8/ 29.6	58.6/31.7	58.9/34.0	58.3/32.6	54.1/27.4
Multi-Agent Scheduling					
Multiple Random	34.5/16.9	60.7/35.1	61.2/37.1	61.4/36.4	58.8/12.9
Full Communication	29.1/10.5	63.7/38.4	64.0/39.9	64.7/41.3	65.1/39.2

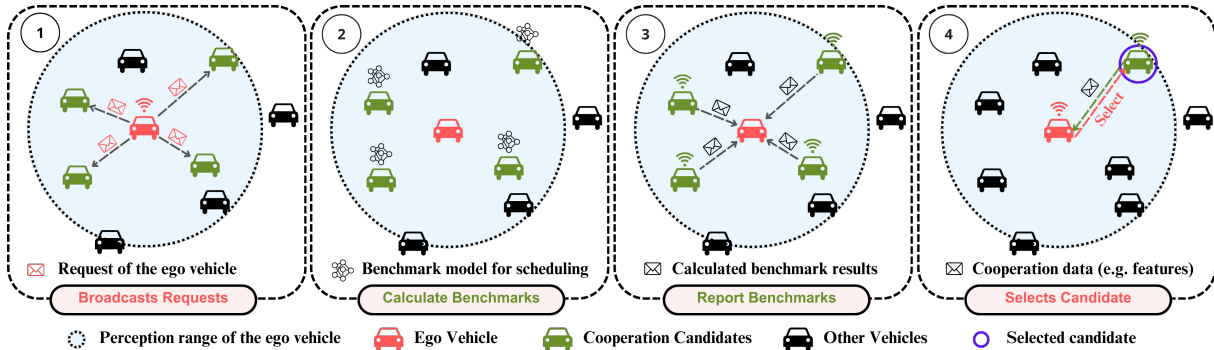


Fig. 4: Visualization of four stages of **agent scheduling**: (1) Ego agent broadcasts requests to cooperative candidate agents. (2) Candidate agents calculate scheduling benchmark with respect to the ego agent. (3) Candidate agents then send these benchmarks back to ego agent. (4) Ego agent selects the candidate agent with the highest benchmark to cooperate with.

location to the candidates, who then calculate the reward based on their historical results and return it to the ego agent.

The results of these experiments are presented in Table VI. In this table, each row corresponds to the scheduling policy used during the inference procedure, while each column corresponds to the same scheduling policy applied during the training procedure. The single-agent scheduling section includes the performances of various policies that ego vehicle selects a single candidate agent for cooperation, while the multi-agent scheduling refers to the algorithms involving the scheduling of two or more agents in CP.

The results show that Historical Best and MASS [27], trained under Single Random agent scheduling policy, deliver the best performance in object detection for single-agent scheduling at both 50m and 100m. Note that some inference results using MASS [27] and Historical Best are identical due to their similarity in utilizing historical agent it has cooperated with. The difference is that in MASS [27], ego agent does not require handshakes to schedule, therefore, it only records the last agent it has cooperated with, while in Historical Best, the ego agent requires handshakes to schedule and thus, it can record all the historical agents it has cooperated with.

In the multi-agent scheduling results, Full Communication outperforms all other training strategies except No Fusion. This is because the model is trained in a stand-alone perception setting, and providing significantly more data during inference will overwhelm the model, introducing noise and leading to a drop in performance.

The scheduling policy plays a less impactful role when

the number of candidates is limited to one or two vehicles in most existing datasets. However, it becomes crucial in our dataset, which features a large number of agents. While most previous datasets focus on CP between a given pair or combination of intelligent agents, our dataset emphasizes on optimizing the scheduling problem in CP. Stochastic training policies outperform deterministic ones by generating more diversified inputs and generalizing better within limited training epochs, regardless of inference policies. Our experimental results show that cooperation and scheduling are of great importance when the detection range increases.

V. CONCLUSIONS

We present WHALES, a multi-agent scheduling dataset containing 17K LiDAR frames, 70K RGB images, and a total of 2.01M 3D annotations, to advance research in V2V cooperative autonomous driving. We enhance CARLA’s simulation speed by synchronizing agent processes for raw data generation batching data processing through a deep learning model. Additionally, we introduce benchmarks for 3D object detection and agent scheduling to showcase the strengths of our dataset. We implement various scheduling algorithms alongside our 3D object detection to evaluate the impact of scheduling on cooperative perception. Our dataset also features controllable agents behaviors, enabling research into agent interaction and control strategies. In the future, we aim to expand cooperation in autonomous driving beyond perception by implementing modular and end-to-end autonomous driving systems using this dataset and evaluating the safety improvements contributed by cooperation.

REFERENCES

- [1] Z. Liu, H. Tang, A. Amini, X. Yang, H. Mao, D. L. Rus, and S. Han, "Befusion: Multi-task multi-sensor fusion with unified bird's-eye view representation," in *2023 IEEE International Conf. on Robotics and Automation (ICRA)*, pp. 2774–2781, IEEE, London, UK, May–Jun. 2023.
- [2] X. Tian, T. Jiang, L. Yun, Y. Mao, H. Yang, Y. Wang, Y. Wang, and H. Zhao, "Occ3d: A large-scale 3d occupancy prediction benchmark for autonomous driving," *Advances in Neural Information Processing Systems*, vol. 36, New Orleans, LA, Dec. 2023.
- [3] T. Meinhardt, A. Kirillov, L. Leal-Taixe, and C. Feichtenhofer, "Trackerformer: Multi-object tracking with transformers," in *Proc. IEEE/CVF conf. on Computer Vision and Pattern Recognition (CVPR)*, pp. 8844–8854, New Orleans, LA, Jun. 2022.
- [4] Y. Hu, J. Yang, L. Chen, K. Li, C. Sima, X. Zhu, S. Chai, S. Du, T. Lin, W. Wang, *et al.*, "Planning-oriented autonomous driving," in *Proc. IEEE/CVF conf. on Computer Vision and Pattern Recognition (CVPR)*, pp. 17853–17862, Vancouver, Canada, Jun. 2023.
- [5] M. H. C. Garcia, A. Molina-Galan, M. Boban, J. Gozalvez, B. Coll-Perales, T. Şahin, and A. Kousaridas, "A tutorial on 5g nr v2x communications," *IEEE Communications Surveys & Tutorials*, vol. 23, no. 3, pp. 1972–2026, Feb. 2021.
- [6] R. Xu, H. Xiang, Z. Tu, X. Xia, M.-H. Yang, and J. Ma, "V2x-vit: Vehicle-to-everything cooperative perception with vision transformer," in *European Conf. on Computer Vision (ECCV)*, pp. 107–124, Springer, Tel Aviv, Israel, Oct. 2022.
- [7] Y. Hu, S. Fang, Z. Lei, Y. Zhong, and S. Chen, "Where2comm: Communication-efficient collaborative perception via spatial confidence maps," *Advances in Neural Information Processing Systems*, vol. 35, pp. 4874–4886, New Orleans, LA, Sep. 2022.
- [8] Z. Lei, S. Ren, Y. Hu, W. Zhang, and S. Chen, "Latency-aware collaborative perception," in *European conf. on Computer Vision (ECCV)*, pp. 316–332, Springer, Tel Aviv, Israel, Oct. 2022.
- [9] J. Li, R. Xu, X. Liu, J. Ma, Z. Chi, J. Ma, and H. Yu, "Learning for vehicle-to-vehicle cooperative perception under lossy communication," *IEEE Transactions on Intelligent Vehicles*, vol. 8, no. 4, pp. 2650–2660, Apr. 2023.
- [10] Y. Hu, Y. Lu, R. Xu, W. Xie, S. Chen, and Y. Wang, "Collaboration helps camera overtake lidar in 3d detection," in *Proc. IEEE/CVF conf. on Computer Vision and Pattern Recognition (CVPR)*, pp. 9243–9252, Vancouver, Canada, Jun. 2023.
- [11] Y. Han, H. Zhang, H. Li, Y. Jin, C. Lang, and Y. Li, "Collaborative perception in autonomous driving: Methods, datasets and challenges," *arXiv preprint arXiv:2301.06262*, Sep. 2023.
- [12] Y. Lu, Q. Li, B. Liu, M. Dianati, C. Feng, S. Chen, and Y. Wang, "Robust collaborative 3d object detection in presence of pose errors," in *2023 IEEE International conf. on Robotics and Automation (ICRA)*, pp. 4812–4818, IEEE, London, England, May–Jun. 2023.
- [13] M. Contributors, "Mmdetection3d: Openmmlab next-generation platform for general 3d object detection," 2020. <https://github.com/open-mmlab/mmdetection3d>.
- [14] A. Geiger, P. Lenz, C. Stillier, and R. Urtasun, "Vision meets robotics: The kitti dataset," *The International Journal of Robotics Research*, vol. 32, no. 11, pp. 1231–1237, Sep. 2013.
- [15] H. Caesar, V. Bankiti, A. H. Lang, S. Vora, V. E. Liong, Q. Xu, A. Krishnan, Y. Pan, G. Baldan, and O. Beijbom, "nuscenes: A multimodal dataset for autonomous driving," in *Proc. IEEE/CVF conf. on Computer Vision and Pattern Recognition (CVPR)*, pp. 11621–11631, Seattle, UAS, Jun. 2020.
- [16] H. Yu, Y. Luo, M. Shu, Y. Huo, Z. Yang, Y. Shi, Z. Guo, H. Li, X. Hu, J. Yuan, *et al.*, "Dair-v2x: A large-scale dataset for vehicle-infrastructure cooperative 3d object detection," in *Proc. IEEE/CVF conf. on Computer Vision and Pattern Recognition (CVPR)*, pp. 21361–21370, New Orleans, LA, Jun. 2022.
- [17] Y. Li, D. Ma, Z. An, Z. Wang, Y. Zhong, S. Chen, and C. Feng, "V2x-sim: Multi-agent collaborative perception dataset and benchmark for autonomous driving," *IEEE Robotics and Automation Letters*, vol. 7, no. 4, pp. 10914–10921, Oct. 2022.
- [18] R. Xu, H. Xiang, X. Xia, X. Han, J. Li, and J. Ma, "Opv2v: An open benchmark dataset and fusion pipeline for perception with vehicle-to-vehicle communication," in *2022 International conf. on Robotics and Automation (ICRA)*, pp. 2583–2589, IEEE, Philadelphia, PA, USA, May 2022.
- [19] R. Mao, J. Guo, Y. Jia, Y. Sun, S. Zhou, and Z. Niu, "Dolphins: Dataset for collaborative perception enabled harmonious and interconnected self-driving," in *Proc. Asian conf. on Computer Vision (ACCV)*, pp. 4361–4377, Macau SAR, China, Dec. 2022.
- [20] R. Xu, X. Xia, J. Li, H. Li, S. Zhang, Z. Tu, Z. Meng, H. Xiang, X. Dong, R. Song, *et al.*, "V2v4real: A real-world large-scale dataset for vehicle-to-vehicle cooperative perception," in *Proc. IEEE/CVF conf. on Computer Vision and Pattern Recognition (CVPR)*, pp. 13712–13722, Vancouver, Canada, Jun. 2023.
- [21] P. Sun, H. Kretschmar, X. Dotiwalla, A. Chouard, V. Patnaik, P. Tsui, J. Guo, Y. Zhou, Y. Chai, B. Caine, *et al.*, "Scalability in perception for autonomous driving: Waymo open dataset," in *Proc. IEEE/CVF conf. on Computer Vision and Pattern Recognition (CVPR)*, pp. 2446–2454, Seattle, WA, USA, Jun. 2020.
- [22] M.-F. Chang, J. Lambert, P. Sangkloy, J. Singh, S. Bak, A. Hartnett, D. Wang, P. Carr, S. Lucey, D. Ramanan, *et al.*, "Argoverse: 3d tracking and forecasting with rich maps," in *Proc. IEEE/CVF conf. on Computer Vision and Pattern Recognition (CVPR)*, pp. 8748–8757, Long Beach, CA, Jun. 2019.
- [23] B. Wilson, W. Qi, T. Agarwal, J. Lambert, J. Singh, S. Khandelwal, B. Pan, R. Kumar, A. Hartnett, J. K. Pontes, *et al.*, "Argoverse 2: Next generation datasets for self-driving perception and forecasting," *arXiv preprint arXiv:2301.00493*, Jun. 2023.
- [24] H. Caesar, J. Kabzan, K. S. Tan, W. K. Fong, E. Wolff, A. Lang, L. Fletcher, O. Beijbom, and S. Omari, "NuPlan: A closed-loop ml-based planning benchmark for autonomous vehicles," *arXiv preprint arXiv:2106.11810*, Jun. 2021.
- [25] H. Yu, W. Yang, H. Ruan, Z. Yang, Y. Tang, X. Gao, X. Hao, Y. Shi, Y. Pan, N. Sun, *et al.*, "V2x-seq: A large-scale sequential dataset for vehicle-infrastructure cooperative perception and forecasting," in *Proc. IEEE/CVF conf. on Computer Vision and Pattern Recognition (CVPR)*, pp. 5486–5495, Vancouver, Canada, Jun. 2023.
- [26] A. Dosovitskiy, G. Ros, F. Codevilla, A. Lopez, and V. Koltun, "Carla: An open urban driving simulator," in *Proc. Ann. conf. on Robot Learning*, pp. 1–16, PMLR, Mountain View, USA, Nov. 2017.
- [27] Y. Jia, R. Mao, Y. Sun, S. Zhou, and Z. Niu, "Mass: Mobility-aware sensor scheduling of cooperative perception for connected automated driving," *IEEE Transactions on Vehicular Technology*, pp. 14962–14977, Nov. 2023.
- [28] Y. Jia, R. Mao, Y. Sun, S. Zhou, and Z. Niu, "Online v2x scheduling for raw-level cooperative perception," in *Proc. IEEE Int. Conf. Commun. (ICC)*, pp. 309–314, IEEE, Seoul, South Korea, May. 2022.
- [29] Z. Zhang, A. Liniger, D. Dai, F. Yu, and L. Van Gool, "End-to-end urban driving by imitating a reinforcement learning coach," in *Proc. IEEE/CVF International Conf. on Computer Vision (ICCV)*, pp. 15222–15232, Montreal, Canada, Oct. 2021.
- [30] R. Xu, Y. Guo, X. Han, X. Xia, H. Xiang, and J. Ma, "OpenCda: An open cooperative driving automation framework integrated with co-simulation," in *2021 IEEE International Intelligent Transportation Systems Conference (ITSC)*, pp. 1155–1162, IEEE, Indianapolis, IN, Sep. 2021.
- [31] A. H. Lang, S. Vora, H. Caesar, L. Zhou, J. Yang, and O. Beijbom, "Pointpillars: Fast encoders for object detection from point clouds," in *Proc. IEEE/CVF conf. on Computer Vision and Pattern Recognition (CVPR)*, pp. 12697–12705, Long Beach, CA, Jun. 2019.
- [32] Y. Yan, Y. Mao, and B. Li, "Second: Sparsely embedded convolutional detection," *Sensors*, vol. 18, no. 10, p. 3337, Oct. 2018.
- [33] I. Radosavovic, R. P. Kosaraju, R. Girshick, K. He, and P. Dollár, "Designing network design spaces," in *Proc. IEEE/CVF conf. on Computer Vision and Pattern Recognition (CVPR)*, pp. 10428–10436, Seattle, WA, USA, Jun. 2020.
- [34] Y. Chen, J. Liu, X. Zhang, X. Qi, and J. Jia, "Voxelnext: Fully sparse voxelnet for 3d object detection and tracking," in *Proceedings of the IEEE/CVF Conference on Computer Vision and Pattern Recognition*, 2023.
- [35] Q. Chen, X. Ma, S. Tang, J. Guo, Q. Yang, and S. Fu, "F-cooper: Feature based cooperative perception for autonomous vehicle edge computing system using 3d point clouds," in *Proceedings of the 4th ACM/IEEE Symposium on Edge Computing*, pp. 88–100, 2019.